Testing primordial non-Gaussianities on galactic scales at high redshift.

M. Habouzit, T. Nishimichi, S. Peirani, G. A. Mamon, J. Silk, J. Chevallard

HAL Id: insu-03645244
https://insu.hal.science/insu-03645244

Submitted on 25 Apr 2022

Testing primordial non-Gaussianities on galactic scales at high redshift

Mélanie Habouzit,[1][*] Takahiro Nishimichi,[1] Sébastien Peirani,[1] Gary A. Mamon,[1]
Joseph Silk[1,2] and Jacopo Chevallard[1]

[1]*Institut d'Astrophysique de Paris (UMR 7095: CNRS & UPMC), 98 bis Bd Arago, F-75014 Paris, France*
[2]*Department of Physics and Astronomy, The Johns Hopkins University Homewood Campus, Baltimore MD 21218, USA*

ABSTRACT

Primordial non-Gaussianities provide an important test of inflationary models. Although the *Planck* cosmic microwave background experiment has produced strong limits on non-Gaussianity on scales of clusters, there is still room for considerable non-Gaussianity on galactic scales. We have tested the effect of local non-Gaussianity on the high-redshift galaxy population by running five cosmological *N*-body simulations down to $z = 6.5$. For these simulations, we adopt the same initial phases, and either Gaussian or scale-dependent non-Gaussian primordial fluctuations, all consistent with the constraints set by *Planck* on cluster scales. We then assign stellar masses to each halo using the halo–stellar mass empirical relation of Behroozi et al. Our simulations with non-Gaussian initial conditions produce halo mass functions that show clear departures from those obtained from the analogous simulations with Gaussian initial conditions at $z \gtrsim 10$. We observe a >0.3 dex enhancement of the low end of the halo mass function, which leads to a similar effect on the galaxy stellar mass function, which should be testable with future galaxy surveys at $z > 10$. As cosmic reionization is thought to be driven by dwarf galaxies at high redshift, our findings may have implications for the reionization history of the Universe.

Key words: methods: numerical – galaxies: evolution – galaxies: general – galaxies: haloes – galaxies: high-redshift – galaxies: luminosity function, mass function.

1 INTRODUCTION

The simplest inflationary models predict a very nearly Gaussian distribution of density perturbations (Gangui et al. 1994; Acquaviva et al. 2003; Maldacena 2003). Primordial non-Gaussianities are therefore an important test of how physics shaped the universe at early times, at energies too high to be probed by laboratory experiments. The departures from Gaussianity at the leading order are characterized by the *bispectrum*, the Fourier counterpart of the three-point correlation function, and models are often classified by the triangular configuration of wavevectors at which the bispectrum has the largest signal.

Most common is the *local*-type non-Gaussianity, for which the bispectrum is maximal when two of the wavenumbers are much greater than the third one (Gangui et al. 1994). The magnitude of the non-Gaussianity of this type can be parametrized (Komatsu & Spergel 2001) by a parameter, f_{NL}, describing the quadratic coupling of the primordial perturbations

$$\zeta(\boldsymbol{x}) = \zeta_G(\boldsymbol{x}) + \frac{3}{5} f_{NL} \left(\zeta_G^2(\boldsymbol{x}) - \left\langle \zeta_G^2(\boldsymbol{x}) \right\rangle \right), \tag{1}$$

where ζ is the curvature perturbations and ζ_G is a Gaussian random field at the same position. Standard single-field inflationary theo-

ries predict $f_{NL} \sim \varepsilon$, where $\varepsilon \ll 1$ is the slow roll parameter, which is independent of scale (Maldacena 2003). The primordial density fluctuations evolve with time, and lead to the collapse of dark matter particles and baryons. A non-Gaussian (nG) initial spectrum of density perturbations will then affect the distribution of baryonic structures. The *Planck* mission, which mapped in detail the cosmic microwave background (CMB) on the full sky, has provided a much stronger constraint on the local non-Gaussianity parameter, $f_{NL} = 2.7 \pm 5.8$ (Planck Collaboration 2013b), than did the previous CMB mission (the *Wilkinson Microwave Anisotropy Probe*, *WMAP*; Bennett et al. 2013).

By appealing to the theory of Press & Schechter (1974), it is straightforward to show that positively skewed ($f_{NL} > 0$) primordial density fluctuations increase the halo mass function (HMF) at large masses with respect to that arising from Gaussian initial conditions (ICs; e.g. Matarrese, Verde & Jimenez 2000). This effect has also been checked with cosmological *N*-body simulations (Grossi et al. 2007; Kang, Norberg & Silk 2007; Pillepich, Porciani & Hahn 2010). Simulations with non-Gaussian initial conditions (nGICs) have been used to probe the HMF (Grossi et al. 2007; Kang et al. 2007; Pillepich et al. 2010), the scale-dependent halo bias (Dalal et al. 2008; Desjacques, Seljak & Iliev 2009; Grossi et al. 2009) and bispectrum (Nishimichi et al. 2010; Sefusatti, Crocce & Desjacques 2010), weak lensing statistics (Pace et al. 2011; Shirasaki et al. 2012) and the pairwise velocity distribution function (Lam, Nishimichi

& Yoshida 2011). Hydrodynamical cosmological simulations have been performed with nGICs to study the baryon history (Maio & Iannuzzi 2011), the gas distribution (Maio 2011), the gas density profiles (Maio & Khochfar 2012) and SZ maps (Pace & Maio 2014).

These studies have all used a scale-independent value of f_{NL}. However, the new constraint on f_{NL} on large scales does not exclude non-Gaussianity on smaller scales, namely galactic scales. Indeed, the non-Gaussianity might depend on scale, as predicted, e.g. in several inflation models with a variable speed of sound, such as the string-based Dirac–Born–Infeld models (Alishahiha, Silverstein & Tong 2004; Silverstein & Tong 2004; Chen 2005).

It is thus possible that significant non-Gaussianity can lurk on the comoving scales of galaxies without being detected by the *Planck* CMB mission, whose angular resolution effectively limits it to the scales of clusters of galaxies. A *blue* spectrum of *running non-Gaussianity* might enhance low masses instead, if the spectrum is blue enough, i.e. if $d\ln f_{NL}/d\ln k$ is large enough. The effects of scale-dependent non-Gaussianity on the HMF (cluster counts) and on reionization were analytically predicted by LoVerde et al. (2008) and Crociani et al. (2009), respectively. Because small scales are still poorly constrained at high redshifts ($z > 6$), cosmological simulations are key for predicting whether non-Gaussianities have an impact on galactic scales. Only one team has run nG simulations with an *explicit scale dependence* adjustable by a free parameter (Shandera, Dalal & Huterer 2011), focusing on halo clustering in the local Universe.

The present work aims to predict, analytically and with cosmological *N*-body simulations, the effects of running non-Gaussianity on the galaxy stellar mass function (SMF), focusing on high redshifts ($z > 6$, i.e. less than 950 Myr after the big bang), where the effects of primordial non-Gaussianity ought to be most important, and on masses low enough that one may see the reverse of the enhancement of the SMF caused by $f_{NL} > 0$, from the high end to the low end. Future galaxy surveys with *Euclid* or the *James Webb Space Telescope* may soon probe these fairly low masses at very high redshifts.

This Letter is organized as follows. In Section 2, we present our simulations, in particular the set-up of the nGICs, as well as our adopted galaxy formation and evolution model. Section 3 begins with an analytical prediction of the HMF arising from nGICs, and then we compare both HMFs and SMFs derived from our simulations with nGICs with those from our Gaussian simulations. Finally, we summarize and discuss our results in Section 4.

2 METHODOLOGY

2.1 Initial conditions: prescription for $f_{NL}(k)$

We employed a simple model that allows a significant amount of non-Gaussianity on small scales, relevant for early structure formation, while keeping such effects small on large scales to meet the strong constraints obtained by the *Planck* CMB mission (Planck Collaboration 2013b). Namely, we investigated here the *generalized local ansatz* proposed by Becker, Huterer & Kadota (2011):

$$\zeta(\boldsymbol{x}) = \zeta_G(\boldsymbol{x}) + \frac{3}{5}\left[f_{NL} \star \left(\zeta_G^2 - \langle\zeta_G^2\rangle\right)\right](\boldsymbol{x}), \quad (2)$$

where the operation $(f_{NL}\star A)$ is the convolution of a random variable A and a k-dependent kernel defined in Fourier space:

$$f_{NL}(k) = f_{NL,0}\left(\frac{k}{k_0}\right)^{\alpha}. \quad (3)$$

We explored four different nG models by varying the normalization $f_{NL,0}$ and the slope $\alpha = d\ln f_{NL}/d\ln k$, in such a way that the non-Gaussianity is significant on galactic scales, yet small enough to meet the current constraints from *Planck* (Planck Collaboration 2013b). Table 1 (normalization and slope for $k_0 = 100\,h\,\mathrm{Mpc}^{-1}$) lists our adopted models, while Fig. 1 displays these models with current constraints from CMB experiments. We restricted ourselves to positively skewed primordial density fluctuations, i.e. $f_{NL} > 0$, and hence $f_{NL,0} > 0$.

We modified the IC generator originally developed by Nishimichi et al. (2009), based on second-order Lagrangian perturbation theory (e.g. Scoccimarro 1998; Crocce, Pueblas & Scoccimarro 2006), parallelized by Valageas & Nishimichi (2011) and with local-type non-Gaussianities implemented by Nishimichi (2012). We followed Becker et al. (2011) and realized the generalized local ansatz of equation (2) by taking a convolution of the curvature squared and the k-dependent f_{NL} kernel in Fourier space. We used the public Boltzmann code, CAMB (Lewis, Challinor & Lasenby 2000), to compute the transfer function and multiply it to the curvature perturbations to have the linear density fluctuations.

2.2 *N*-body simulations and halo catalogue

We have performed five cosmological simulations with GADGET-2 (Springel 2005) for a Λ cold dark matter universe using *Planck* parameters (Planck Collaboration 2013a), namely $\Omega_M = 0.307$, $\Omega_\Lambda = 0.693$, $h = 0.678$ and $\sigma_8 = 0.829$. Each simulation was performed in a periodic box of side $50\,h^{-1}$ Mpc with 1024^3 dark matter particles (e.g. with mass resolution of $\sim 9.9 \times 10^6\,h^{-1}\,M_\odot$).

Table 1. Characteristics of f_{NL} models (equation 3).

Model	G	NG1	NG2	NG3	NG4
$f_{NL,0}$	0	82	1000	7357	10 000
α	–	1/2	4/3	2	4/3
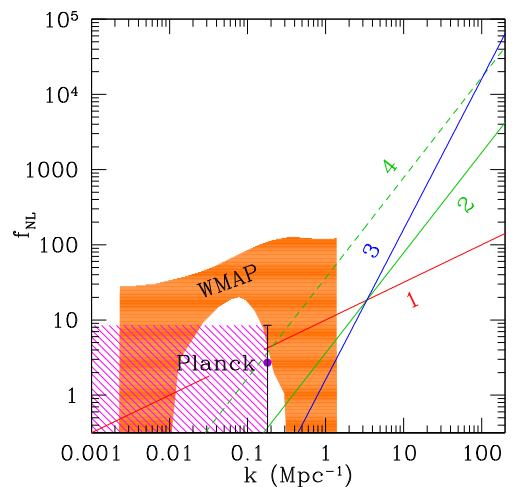
Figure 1. Models (lines) for the scale-dependent nG parameter $f_{NL}(k)$ (equation 3, with parameters listed in Table 1). The orange shaded region represents the allowed values from *WMAP*, within 1σ, of $f_{NL}(k)$ according to Becker & Huterer (2012). The magenta shaded region shows the *Planck* constraint (Planck Collaboration 2013b). The right edge of the box corresponds to a scale of $2\pi/k \simeq 30$ kpc, i.e. the scales of galaxies are to the right of the right edge of the box.

One simulation (hereafter 'G') started with Gaussian ICs, while the other four (hereafter 'NG') began with nGICs (equations 2 and 3, with parameters in Table 1), with the same initial phases. The simulations started at $z = 200$ and ended at $z = 6.5$. In each case, the Plummer-equivalent force softening was set to 5 per cent of the mean interparticle distance ($2.44 \, h^{-1}$ kpc in comoving units).

For each snapshot (taken every ~ 40 Myr), catalogues of haloes were prepared using ADAPTAHOP (Aubert, Pichon & Colombi 2004), which employs a smoothed particle hydrodynamics-like kernel to compute densities at the location of each particle and partitions the ensemble of particles into (sub)haloes based on saddle points in the density field. Only haloes or subhaloes containing at least 20 particles (e.g. $2.9 \times 10^8 \, M_\odot$) were retained. We then studied the individual evolution of (sub)haloes, by building halo merger trees using TREEMAKER (Tweed et al. 2009), which allowed us to accurately derive the mass evolution of each dark matter (sub)halo. This was the basis to compute the evolution of galaxy stellar masses, as we shall see in Section 2.3.

2.3 Galaxy formation and evolution model

Galaxy stellar masses are 'painted' on the haloes and subhaloes using the Behroozi, Wechsler & Conroy (2013) model that provides the galaxy mass m as a function of halo mass M and redshift z. We could have adopted a *physical* model, such as Cattaneo et al. (2011). We also considered using the *empirical* model of Mutch, Croton & Poole (2013). The former model is only constrained at $z = 0$, while the latter extends to $z = 4$, which is still insufficient for our purposes. We have thus preferred to adopt the empirical model of Behroozi et al., whose parameters were fitted to the galaxy SMFs, specific star formation rates and cosmic star formation rate, from $z = 0$ to 8. In particular, the Behroozi et al. model is the only empirical model of galaxy mass versus halo mass and redshift that extends up to the redshift when reionization is thought to occur. A weakness of our approach is that, for lack of a better simple model, we assume that the Behroozi et al. model can be extrapolated beyond $z = 8$ to 17.

The Behroozi et al. model was calibrated with HMFs derived from cosmological simulations with Gaussian ICs. One could argue that their model cannot be applied to simulations with nGICs, without appropriate corrections. Alternatively, one could adopt the Behroozi et al. model as a basis to which we can compare the effects of Gaussian versus non-Gaussian ICs, and this is what we do here.

However, we slightly modify the Behroozi et al. model, by preventing galaxy masses from decreasing in time. For quiescent (sub)haloes, we simply apply $m(M, z)$, while for merging (sub)haloes, we compare the galaxy mass $m(M, z)$ to the sum over all its progenitors (in the previous timestep). If the galaxy mass from the model is higher than the sum of progenitor masses, we apply $m(M, z)$; if the galaxy mass is smaller, the new galaxy mass is the sum over all its progenitors.

3 RESULTS

3.1 Predicted halo mass functions from theory

Before discussing the results of our numerical simulations, it is worth presenting analytical predictions to gain insight into the potential consequences of scale-dependent non-Gaussianities on early structure formation. We here adopt a simple model and discuss the effects on the HMF.

We follow the Press–Schechter formalism (Press & Schechter 1974) for this calculation. Namely, we work with the linear density

field, δ_M, smoothed with a spherical top-hat window that encompasses a mass M and linearly extrapolated to $z = 0$, and consider that the one-point cumulants of this field uniquely determine the HMF. Assuming that the nG correction is small, we apply the Edgeworth expansion to the one-point density probability distribution function (LoVerde et al. 2008). Up to the skewness order, the nG to Gaussian ratio of the HMF is given by

$$\frac{\mathrm{d}n_{\mathrm{nG}}/\mathrm{d}M}{\mathrm{d}n_{\mathrm{G}}/\mathrm{d}M}(M, z) = 1 + \frac{1}{6} C_M^{(3)} H_3(\nu) + \frac{1}{6} \frac{\mathrm{d}C_M^{(3)}}{\mathrm{d}\ln\sigma_M} \frac{H_2(\nu)}{\nu}, \quad (4)$$

where $\sigma^2(M) = \langle \delta_M^2 \rangle$ is the variance of the density fluctuations δ_M, $C_M^{(3)} = \langle \delta_M^3 \rangle / \sigma_M^3$ is a measure of the skewness of δ_M, $\nu = \delta_c(z)/\sigma(M)$ is the peak height, given $\delta_c(z) = 1.686/D_+(z)$, the threshold density contrast for spherical collapse at redshift z, where $D_+(z)$ is the growth rate, and finally H_n is the Hermite polynomial.

In this model, all the nG correction comes from the skewness, which can be expressed by an integral of the *bispectrum*:

$$\langle \delta_M^3 \rangle = \int \frac{\mathrm{d}^3 \boldsymbol{p} \, \mathrm{d}^3 \boldsymbol{q}}{(2\pi)^6} \mathcal{M}(p) \mathcal{M}(q) \mathcal{M}(|\boldsymbol{p} + \boldsymbol{q}|) B_\zeta(p, q, |\boldsymbol{p} + \boldsymbol{q}|), \quad (5)$$

where $\mathcal{M}$ stands for the transfer function from the curvature to the density fluctuation smoothed by a mass scale M, and the bispectrum of the curvature ζ in the model (2) is given by

$$B_\zeta(k_1, k_2, k_3) = \frac{6}{5} \left[f_{\mathrm{NL}}(k_1) P_\zeta(k_2) P_\zeta(k_3) + (\mathrm{cyc.}\, 2) \right], \quad (6)$$

where (cyc. 2) denotes two more terms that are obtained by cyclic permutation of the wavenumbers in the first term. The k-dependence of f_{NL} propagates to the mass dependence of skewness through these equations, making the nG correction to the HMF rather non-trivial. Since we focus on blue f_{NL} (i.e. $\alpha > 0$), we anticipate that the correction to the HMF gets larger at low masses.

Fig. 2 shows the analytical prediction (equation 4) at $z = 10$ (left) and $z = 7$ (right). We here adopt $k_0 = 5.11 \, h$ Mpc^{-1}, $f_{\mathrm{NL}, 0} = 18.5$, which is the intersection of the models 1, 2 and 3 (see Fig. 1), and vary the slope α as indicated in the figure legend. There are two noticeable trends in Fig. 2. First, the dependence of the HMF ratio on M depends on the slope α: the boost from non-Gaussianity is an increasing function of M for $\alpha < 1$, while a larger α results in a decreasing function of M. This high-mass enhancement of the HMF for small α is consistent with LoVerde et al. (2008). Because of the ν-dependence in equation (4), rare objects receive more nG effect in these cases. When the k-dependence of f_{NL} is blue enough, it is
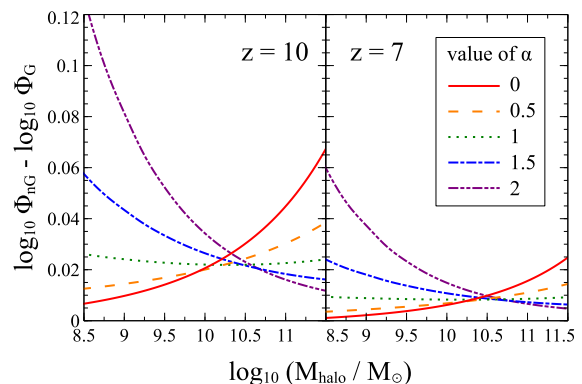
Figure 2. Analytical predictions of the nG correction to the HMF. We plot the ratio of the HMF with non-Gaussian and Gaussian ICs at $z = 10$ (left) and $z = 7$ (right), for different running $f_{\mathrm{NL}}(k)$ passing through the pivot point of the first three models of Table 1 (see Fig. 1).
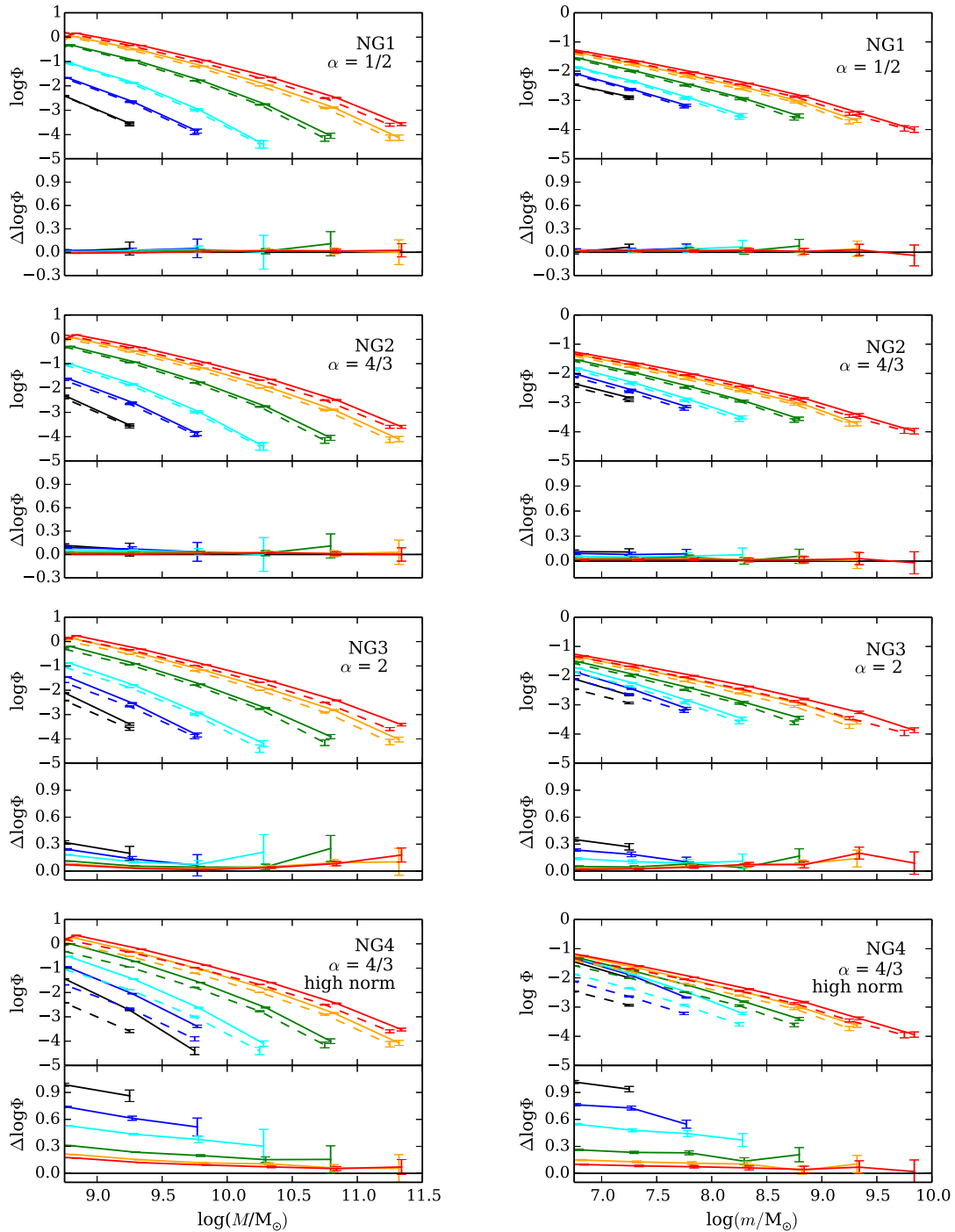
Figure 3. Upper panels of boxes: halo (left) and galaxy stellar (right) mass functions (in Mpc^{-3} dex^{-1}) for different ICs: Gaussian models (dashed) and non-Gaussian models 1–4 (from top to bottom). Lower panels of boxes: residuals of the log mass function relative to that of the Gaussian run (the horizontal line shows equal non-Gaussian and Gaussian mass functions). The errors are Poisson. The different curves indicate different redshifts (decreasing upwards for the large boxes): $z = 17$ (black), $z = 15$ (blue), $z = 13$ (cyan), $z = 10$ (green), $z = 8$ (orange) and $z = 7$ (red).

the low-mass end of the HMF that is enhanced, so that the mass dependence in $C_M^{(3)}$ overwhelms that of $H_3(\nu)$. Secondly, the nG correction is more prominent at higher redshift. It is about a factor of 2 greater at $z = 10$ compared to $z = 7$. However, not shown here, structure formation at low redshift is almost unaffected with the models that we consider here (i.e. the change of dn/dM is less than 10 per cent at $z < 3$ over the mass range shown in Fig. 2). Thus, early structure formation provides us with a unique opportunity

to constrain scale-dependent non-Gaussianity, given the very tight *Planck* constraints on large scales.

3.2 Results from simulations

The left-hand panels of Fig. 3 show the HMFs obtained from the five cosmological simulations. One sees (upper-left panel of Fig. 3) that the effects of non-Gaussianity on the HMF are increasingly

important with increasing model number (see for example the upper-left panel of Fig. 3).

Non-Gaussian models NG1 ($\alpha = 1/2$) and NG2 ($\alpha = 4/3$, low normalization) cause only small (less than 0.1 dex) and insignificant enhancements of the HMF (top two left-hand panels of Fig. 3) and SMF (top two right-hand panels of Fig. 3). Non-Gaussian model NG3, with a very steep slope ($\alpha = 2$), produces significant enhancements (left-hand panel in third row of Fig. 3) of up to 0.3 dex ($z = 17$) or 0.2 dex ($z = 15$), in the HMF at $\log M/M_\odot = 9$. Finally, model NG4, with a slope 4/3 but a much higher normalization (10 times that of model NG2), produces very large enhancements of the HMFs and SMFs at low masses and high redshifts: greater than 0.3 dex enhancements in the HMF arise for $z \geq 13$ at all halo masses and $z \geq 10$ for $\log M/M_\odot < 9.5$. The corresponding SMF is also enhanced by over 0.3 dex for all galaxy masses at $z \geq 13$ and at galaxy masses $\log m/M_\odot \leq 6.8$ for $z = 10$.

4 CONCLUSIONS AND DISCUSSION

The results presented here indicate that, in comparison with the predictions from Gaussian ICs, simulations with ICs that are increasingly non-Gaussian at smaller scales, yet consistent with the CMB constraints from *Planck*, can lead to small, but eventually detectable alterations to the halo and galaxy SMFs. Since constant $f_{NL} > 0$ enhances the HMF principally at large masses, one can think that low slopes of $\alpha = \mathrm{d}\ln f_{NL}/\mathrm{d}\ln k > 0$ (keeping $f_{NL} > 0$) should also enhance the high-mass end of the HMF, while a high enough slope should do the opposite and enhance the HMF at the low-mass end. At $\alpha = 2$, the HMF is in fact enhanced, both at the high and low ends (left residual plot of third row of Fig. 3, although that of the high end is only marginally significant). However, for the shallower slope ($\alpha = 4/3$), the HMF is only enhanced at the low end. We find that our two strongest nG models (NG3, NG4) exhibit the largest differences, up to 0.2 dex for NG3 ($\alpha = 2$), and greater than 0.3 dex (at $z = 10$) for NG4 ($\alpha = 4/3$, $f_{NL,0} = 10\,000$). These effects of nGICs on our simulated HMFs are close to the theoretical predictions, with some quantitative differences.

Unfortunately, it is difficult to measure the HMF with great accuracy and considerably easier to measure the SMF. We used the state-of-the-art model of stellar mass versus halo mass and redshift of Behroozi et al. (2013) to produce galaxy masses on the (sub)haloes of our cosmological *N*-body simulations. We slightly altered the model to consider halo mergers and prevent galaxy masses from decreasing in time. Comparing the resultant galaxy mass functions of our nG models with that of our Gaussian model, we find similar behaviour of the enhancements of the galaxy mass function with mass and redshift, i.e. 0.2 dex for NG3 and 0.3 dex (at $z = 10$) for NG4.

The modification of the SMF by nGICs can have profound consequences. In particular, the reionization of the Universe by the first stars and galaxies will be affected, in a different way depending on the slope α. Low-mass galaxies are thought to be one of the most powerful sources of ionizing photons at high redshift (Robertson et al. 2013; Wise et al. 2014). Using a set of cosmological simulations, we have seen that faint galaxies are the most affected by primordial non-Gaussianities (see models NG3 with $\alpha = 2$ and NG4 with $\alpha = 4/3$, but high normalization). Therefore, primordial nG perturbations can then strongly affect the thermal history of the intergalactic medium. Effects on the far-UV luminosity function and the reionization history will be discussed in detail in a forthcoming article (Chevallard et al., in preparation).

REFERENCES

Acquaviva V., Bartolo N., Matarrese S., Riotto A., 2003, Nucl. Phys. B, 667, 119
Alishahiha M., Silverstein E., Tong D., 2004, Phys. Rev. D, 70, 123505
Aubert D., Pichon C., Colombi S., 2004, MNRAS, 352, 376
Becker A., Huterer D., 2012, Phys. Rev. Lett., 109, 121302
Becker A., Huterer D., Kadota K., 2011, J. Cosmol. Astropart. Phys., 1, 6
Behroozi P. S., Wechsler R. H., Conroy C., 2013, ApJ, 770, 57
Bennett C. L. et al., 2013, ApJS, 208, 20
Cattaneo A., Mamon G. A., Warnick K., Knebe A., 2011, A&A, 533, A5
Chen X., 2005, Phys. Rev. D, 72, 123518
Crocce M., Pueblas S., Scoccimarro R., 2006, MNRAS, 373, 369
Crociani D., Moscardini L., Viel M., Matarrese S., 2009, MNRAS, 394, 133
Dalal N., Doré O., Huterer D., Shirokov A., 2008, Phys. Rev. D, 77, 123514
Desjacques V., Seljak U., Iliev I. T., 2009, MNRAS, 396, 85
Gangui A., Lucchin F., Matarrese S., Mollerach S., 1994, ApJ, 430, 447
Grossi M., Dolag K., Branchini E., Matarrese S., Moscardini L., 2007, MNRAS, 382, 1261
Grossi M., Verde L., Carbone C., Dolag K., Branchini E., Iannuzzi F., Matarrese S., Moscardini L., 2009, MNRAS, 398, 321
Kang X., Norberg P., Silk J., 2007, MNRAS, 376, 343
Komatsu E., Spergel D. N., 2001, Phys. Rev. D, 63, 063002
Lam T. Y., Nishimichi T., Yoshida N., 2011, MNRAS, 414, 289
Lewis A., Challinor A., Lasenby A., 2000, ApJ, 538, 473
LoVerde M., Miller A., Shandera S., Verde L., 2008, J. Cosmol. Astropart. Phys., 4, 14
Maio U., 2011, Class. Quantum Grav., 28, 225015
Maio U., Iannuzzi F., 2011, MNRAS, 415, 3021
Maio U., Khochfar S., 2012, MNRAS, 421, 1113
Maldacena J., 2003, J. High Energy Phys., 5, 13
Matarrese S., Verde L., Jimenez R., 2000, ApJ, 541, 10
Mutch S. J., Croton D. J., Poole G. B., 2013, MNRAS, 435, 2445
Nishimichi T., 2012, J. Cosmol. Astropart. Phys., 8, 37
Nishimichi T. et al., 2009, PASJ, 61, 321
Nishimichi T., Taruya A., Koyama K., Sabiu C., 2010, J. Cosmol. Astropart. Phys., 7, 2
Pace F., Maio U., 2014, MNRAS, 437, 1308
Pace F., Moscardini L., Bartelmann M., Branchini E., Dolag K., Grossi M., Matarrese S., 2011, MNRAS, 411, 595
Pillepich A., Porciani C., Hahn O., 2010, MNRAS, 402, 191
Planck Collaboration, 2013a, preprint (arXiv:1303.5076)
Planck Collaboration, 2013b, preprint (arXiv:1303.5084)
Press W. H., Schechter P., 1974, ApJ, 187, 425
Robertson B. E. et al., 2013, ApJ, 768, 71
Scoccimarro R., 1998, MNRAS, 299, 1097
Sefusatti E., Crocce M., Desjacques V., 2010, MNRAS, 406, 1014
Shandera S., Dalal N., Huterer D., 2011, J. Cosmol. Astropart. Phys., 3, 17
Shirasaki M., Yoshida N., Hamana T., Nishimichi T., 2012, ApJ, 760, 45
Silverstein E., Tong D., 2004, Phys. Rev. D, 70, 103505
Springel V., 2005, MNRAS, 364, 1105
Tweed D., Devriendt J., Blaizot J., Colombi S., Slyz A., 2009, A&A, 506, 647
Valageas P., Nishimichi T., 2011, A&A, 527, A87
Wise J. H., Demchenko V. G., Halicek M. T., Norman M. L., Turk M. J., Abel T., Smith B. D., 2014, MNRAS, 442, 2560

This paper has been typeset from a TEX/LATEX file prepared by the author.